PROCEEDINGS OF SCIENCE

Investigating the puzzling radio structures of the gamma-ray binary LS 5039

E. Molina[a,*] **and V. Bosch-Ramon**[a]

[a] *Departament de Física Quàntica i Astrofísica, Institut de Ciències del Cosmos (ICCUB), Universitat de Barcelona (IEEC-UB),*
Martí i Franquès 1, 08028 Barcelona, Spain

E-mail: emolina@fqa.ub.edu

LS 5039 is a gamma-ray binary system hosting a compact object and a massive O-type stellar companion. It presents a broadband emission spectrum that goes from radio up to gamma rays with energies of a few dozen TeV. In one of the proposed physical scenarios, the compact object is a non-accreting pulsar and the non-thermal radiation comes from an outflow produced by the interaction of the pulsar and stellar winds. We present a semi-analytical model that computes the dynamical evolution of this outflow, as well as its expected non-thermal emission. We compare the model results with the existent data of LS 5039, paying special attention to the extended and time-dependent radio structures observed in the source.

7th Heidelberg International Symposium on High-Energy Gamma-Ray Astronomy (Gamma2022)
4-8 July 2022
Barcelona, Spain

*Speaker

PoS(Gamma2022)064

1. Introduction

LS 5039 is a gamma-ray binary system consisting of a main sequence O-type star and a compact companion of unclear nature. A black hole is favored for low system inclinations ($i \lesssim 30°$), whereas higher inclinations favor a neutron star. Inclinations above $\approx 60°$ are unlikely due to the absence of X-ray eclipses in this system [1]. According to the latest *Gaia* DR3 data, LS 5039 is located at a distance of $d = 2.04 \pm 0.06$ kpc [2]. As reported by [1] in their study of the He II lines, and assuming a system inclination around 50° for the sake of simplicity, the source has an elliptical orbit with a semi-major axis of $a \approx 2.4 \times 10^{12}$ cm, an eccentricity of $e = 0.35 \pm 0.04$, and a period of $T = 3.90603 \pm 0.00017$ days. The superior (SUPC) and inferior (INFC) conjunctions of the compact object correspond, respectively, to orbital phases of $\phi = 0.058$ and 0.716, with $\phi = 0$ corresponding to the periastron. The star has a luminosity of $L_\star = (7 \pm 1) \times 10^{38}$ erg s^{-1}, a radius of $R_\star = 9.3 \pm 0.7$ R$_\odot$, and an effective temperature of $T_\star = (3.9 \pm 0.2) \times 10^4$ K [1] (we note that these parameters were derived using a larger distance of 2.5 kpc). If the compact object is a pulsar, the lack of thermal X-ray emission in the shocked stellar wind puts an upper limit in the pulsar spin-down luminosity of $L_\mathrm{p} \leq 6 \times 10^{36}$ erg s^{-1} [3]. Among the broad multiwavelength spectrum of LS 5039, which ranges from radio up to gamma rays, the extended radio emission is especially interesting. This is so because of the observed variation for different orbital phases, both in morphology and overall flux [4, 5], which points to the existence of non-trivial changes in the emission and/or absorption processes along the orbit.

In these proceedings, we study the multiwavelength emission of LS 5039 in a pulsar-wind scenario. This means that we assume that the compact object is a pulsar and that the interaction between the stellar and pulsar winds produces shocks that accelerate charged particles, which are the responsible of the non-thermal emission observed in the system. This scenario is adopted by a number of recent works [e.g., 6–10], but we note that a microquasar scenario (with either a neutron star or a black hole as a compact object) cannot be ruled out [e.g., 11–13]. Section 2 of these proceedings explains the model used to compute the expected emission from LS 5039, while in Sect. 3 we show the obtained results, compare them with the existing observations of the source, and provide a brief discussion.

2. Model description

In this section, we qualitatively describe the model used to try to reproduce the emission features of LS 5039, both from a dynamical and a radiative point of view. A more detailed explanation of a similar approach can be found in [9]. Primed quantities refer to the frame moving with the outflow fluid.

In our semi-analytical model, the star is located at the origin of the coordinate system. The studied outflow consists of a core of shocked pulsar wind surrounded by a shell of shocked stellar wind, everything confined by the action of the unshocked stellar wind. Close to the binary, this outflow is approximately directed in the star-pulsar direction, although slightly bent in the direction opposite to the orbital motion due to the non-radial component of the stellar wind in the reference frame rotating with the pulsar. Farther away from the system, the outflow takes a spiral-like shape due to the asymmetric interaction with the stellar wind arising from the orbit-related Coriolis forces.

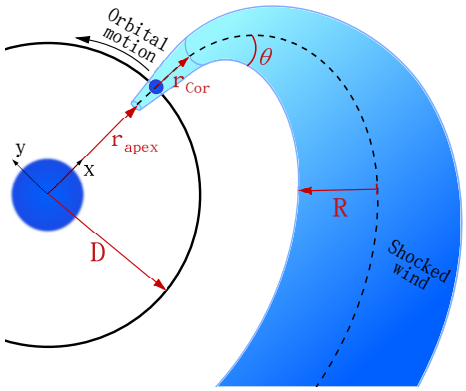

Figure 1: Schematic view of the pulsar-wind scenario adopted for LS 5039 (not to scale). Only a part of the orbit is shown for clarity.

This behavior is shown by numerical hydrodynamic simulations [see, e.g., 14], and is sketched in Fig. 1.

In order to compute the evolution of the outflow, we divide it in segments and take into account that each of them is injected at a different orbital phase. We then let the segments evolve moving away from the binary system, as they get transferred momentum through the asymmetric interaction with the stellar wind. The evolution of the dynamical properties of the segments are computed through conservation equations. We note that this approach is valid roughly for the first turn of the spiral, since farther away wind mixing and instability development start playing an important role [e.g., 14].

The non-thermal emission of the outflow is computed following two different approaches, one of them focused on the point-like emission of the source at X-rays and higher energies, and the other one devoted to the computation of the extended radio emission. In both cases, the emitter is considered to be the inside part of the previously defined outflow, which mainly consists of shocked pulsar material. Therefore, no contribution to the outflow emission from the unshocked wind material is taken into account (see [15] for a study of the potential contribution from the unshocked pulsar wind) . We assume a leptonic origin of the radiation and neglect the hadronic contribution, although the latter may be relevant in some cases (e.g., [16], for a review in the similar case of microquasars jets).

Regarding the high-energy part of the spectrum, the emitter consists of two particle-accelerating sites, one at the point where the pulsar and stellar winds collide frontally, and the other one at the Coriolis turnover, where orbital effects start dominating the outflow trajectory. Electrons (and positrons) accelerated in these two locations move along the outflow as they cool down via adiabatic, synchrotron and inverse Compton processes, the latter two being also responsible for the non-thermal emission of the outflow. Relativistic beaming and gamma-gamma absorption effects are also considered. For discussion purposes, the study of the source emission is divided into two regions: an inner region covering the space between the two accelerators, and an outer region beyond the Coriolis turnover.

For the study of the radio emission of LS 5039, the assumption of the presence of only the 2 accelerators mentioned above is not suitable, since this makes the emission very concentrated around

Table 1: Parameters used for the study of LS 5039.

	Parameter	Value
Star	Temperature $T_\star$	4×10^4 K
	Luminosity $L_\star$	7×10^{38} erg s^{-1}
	Mass-loss rate $\dot{M}_\mathrm{w}$	1.5×10^{-7} M$_\odot$ yr^{-1}
	Wind speed v_w	3×10^8 cm s^{-1}
Pulsar	Luminosity L_p	3×10^{36} erg s^{-1}
	Wind Lorentz factor Γ_p	10^5
System	Orbit semi-major axis a	2.4×10^{12} cm
	Orbital period T	3.9 days
	Orbital eccentricity e	0.35
	Distance to the observer d	2.1 kpc
	1st accel. NT fraction η_NT^A	0.03
	2nd accel. NT fraction η_NT^B	0.18
	Injection power-law index p	-1.3
	Magnetic fraction η_B	0.02
	System inclination i	40°, 60°

the binary system, contradicting the observations of extended radio structures in the source. For this reason, a different method is used. Each of the outflow segments contains an energy $E'_\mathrm{NT} = \eta_\mathrm{NT} U'$ in the form of non-thermal particles, where $\eta_\mathrm{NT} \leq 1$ is an efficiency factor, $U' = V'P/(\gamma - 1)$ is the internal energy of the segment, V' is its proper volume, P is its pressure, and $\gamma = 4/3$ is the adiabatic index of the (relativistic) fluid. The energy E'_NT is used as the normalization for the distribution of the non-thermal electrons at each segment, which is assumed to follow a power-law, $N'(E') \propto E'^p$. This assumption is valid since we focus on the low-energy electrons (responsible for the radio emission through their synchrotron cooling), for which the dynamic energy losses dominate and, therefore, the electron distribution keeps the same shape as the injected one. Once the electron distribution along the outflow is known, its radio output is obtained by computing the synchrotron emission of these electrons. This is done by parametrizing the magnetic field through the fraction η_B of its energy-density relative to the total outflow one, $B'^2/8\pi = \eta_B L_\mathrm{p}/\pi R^2 v \Gamma^2$, where R is the emitter radius, v is the fluid speed, and Γ its Lorentz factor. The intrinsic synchrotron emission is then absorption-corrected through the mechanisms of synchrotron self-absorption and free-free absorption in the stellar wind. Finally, the emission is Doppler (de)boosted by assuming a system inclination of $i = 60°$ and using the corresponding Lorentz factor of the fluid at each segment, obtained from their dynamical evolution.

3. Results and discussion

Figure 2 shows the spectral energy distribution (SED) and light curves (LCs) of LS 5039 predicted by our model for X-ray and higher energies, together with observational data at different energies. These results are obtained using the parameters listed in Table 1, which are found to approximately reproduce the observations. We note that this parameter combination is just an illustrative situation and not a fit to the data, since the degeneracy present for different sets of poorly-constrained free parameters makes performing a statistical analysis not useful. In general, adopting

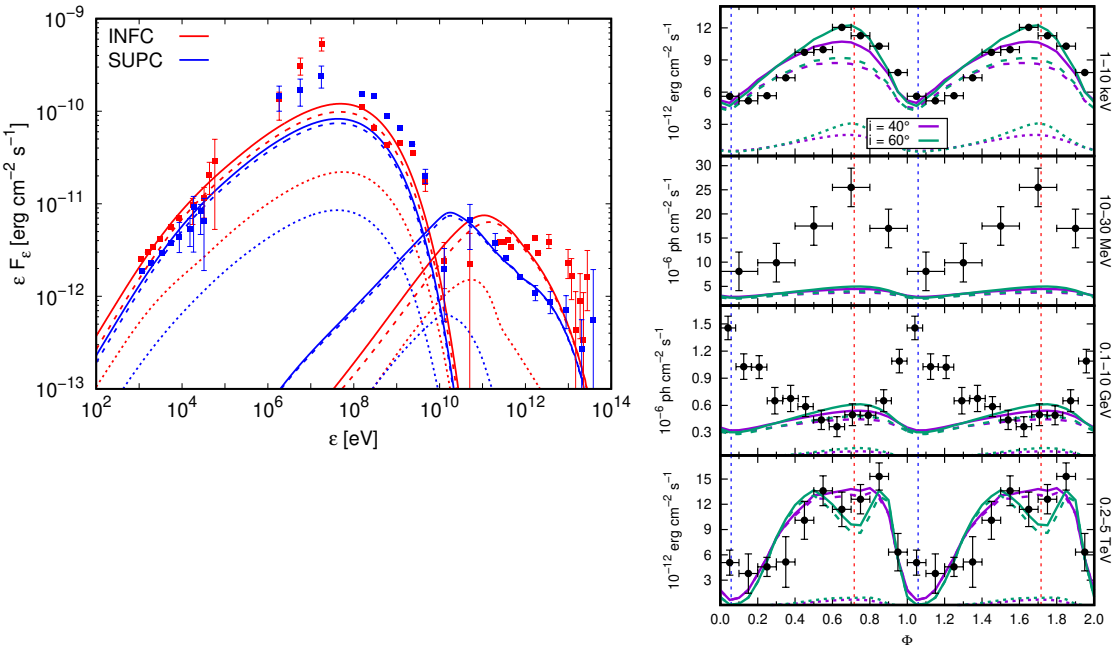

Figure 2: Left panel: Synchrotron and IC SEDs of LS 5039 for $i = 60°$, averaged over the INFC (red lines; $0.45 < \phi \leq 0.90$) and SUPC (blue lines; $0.90 < \phi$ or $\phi \leq 0.45$) phase intervals. The contribution of the inner and outer regions are represented by dotted and dashed lines, respectively. Data from *Suzaku*, COMPTEL, *Fermi*/LAT, and H.E.S.S. are also represented as filled squares. Right panel, from top to bottom: Light curves of LS 5039 in the *Suzaku* (1–10 keV), COMPTEL (10–30 MeV), *Fermi*/LAT (0.1–10 GeV), and H.E.S.S. (0.2–5 TeV) energy ranges, for $i = 40°$ (purple lines) and 60° (green lines). Dotted and dashed lines show the contributions of the inner and outer regions, respectively. The phases corresponding to the INFC (SUPC) are represented with red (blue) vertical dashed lines. See [9] for the references to the different data sets used.

a higher non-thermal energy budget for the 2nd accelerator reproduces better the observations in X- and gamma rays. The X-ray ($\sim$ 10 keV) and very-high-energy gamma-ray ($\gtrsim$ 100 GeV) emission and modulation of LS 5039 is generally well reproduced by the model, especially for high inclinations. The magnitude of the high-energy gamma-ray emission ($\sim$ 1 GeV) is approximately well explained, although not its modulation, with the fluxes being overpredicted (underpredicted) for the INFC (SUPC). Finally, the $\sim$ 10 MeV emission cannot be reproduced by our model, being underpredicted by a factor of up to 5, and likely requires the inclusion of other processes for its proper explanation [e.g., 17].

In Fig. 3, the preliminary simulated radio sky maps at 5 GHz of LS 5039 are shown for generic values of $\eta_{\rm NT} = 0.1$, $p = 2$, $\eta_B = 0.001$, and $i = 60°$. The rest of the parameters are the same as those listed in Table 1. The sky maps show a varying emission for different orbital phases, both in absolute flux and morphology. These features resemble what has been observed [4], which may indicate that we are in the right path regarding the approach used in our model to compute the radio emission of LS 5039. Furthermore, once the model is refined, the radio maps could potentially be used to discriminate between the pulsar-wind and microquasar scenarios for the source.

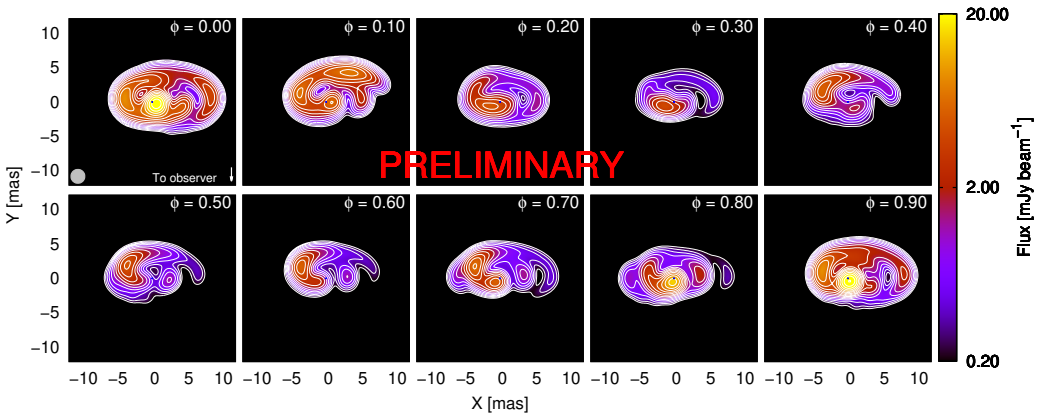

Figure 3: Simulated radio sky maps at 5 GHz for $i = 60°$ and different orbital phases. The assumed telescope beam is shown as a gray circle with a 2-mas diameter in the bottom left corner of the first plot. The contour lines start at a flux of 0.2 mJy beam^{-1} and increase with a factor of $\sqrt{2}$.

Acknowledgments

The authors acknowledge financial support from the State Agency for Research of the Spanish Ministry of Science and Innovation (MCIN/AEI) under grant PID2019-105510GB-C31/AEI/10.13039/501100011033, and through the "Unit of Excellence María de Maeztu 2020-2023" award to the Institute of Cosmos Sciences (CEX2019-000918-M). EM acknowledges support from MCIN through grant BES-2016-076342. VBR is Correspondent Researcher of CONICET, Argentina, at the IAR.

References

[1] J. Casares, M. Ribó, I. Ribas, J.M. Paredes, J. Martí and A. Herrero, *A possible black hole in the γ-ray microquasar LS 5039*, *MNRAS* **364** (2005) 899 [astro-ph/0507549].

[2] C.A.L. Bailer-Jones, J. Rybizki, M. Fouesneau, M. Demleitner and R. Andrae, *Estimating Distances from Parallaxes. V. Geometric and Photogeometric Distances to 1.47 Billion Stars in Gaia Early Data Release 3*, *AJ* **161** (2021) 147 [2012.05220].

[3] V. Zabalza, V. Bosch-Ramon and J.M. Paredes, *Thermal X-Ray Emission from the Shocked Stellar Wind of Pulsar Gamma-Ray Binaries*, *ApJ* **743** (2011) 7 [1108.4269].

[4] J. Moldón, M. Ribó and J.M. Paredes, *Periodic morphological changes in the radio structure of the gamma-ray binary LS 5039*, *A&A* **548** (2012) A103 [1209.6073].

[5] B. Marcote, M. Ribó, J.M. Paredes and C.H. Ishwara-Chandra, *Physical properties of the gamma-ray binary LS 5039 through low- and high-frequency radio observations*, *MNRAS* **451** (2015) 59 [1504.07253].

[6] V. Zabalza, V. Bosch-Ramon, F. Aharonian and D. Khangulyan, *Unraveling the high-energy emission components of gamma-ray binaries*, *A&A* **551** (2013) A17 [1212.3222].

[7] G. Dubus, A. Lamberts and S. Fromang, *Modelling the high-energy emission from gamma-ray binaries using numerical relativistic hydrodynamics*, *A&A* **581** (2015) A27 [1505.01026].

[8] H. Yoneda, K. Makishima, T. Enoto, D. Khangulyan, T. Matsumoto and T. Takahashi, *Sign of Hard-X-Ray Pulsation from the γ -Ray Binary System LS 5039*, *Phys. Rev. Lett.* **125** (2020) 111103 [2009.02075].

[9] E. Molina and V. Bosch-Ramon, *A dynamical and radiation semi-analytical model of pulsar-star colliding winds along the orbit: Application to LS 5039*, *A&A* **641** (2020) A84 [2007.00543].

[10] D. Huber, R. Kissmann and O. Reimer, *Relativistic fluid modelling of gamma-ray binaries. II. Application to LS 5039*, *A&A* **649** (2021) A71 [2103.00995].

[11] M.V. McSwain and D.R. Gies, *Wind Accretion and Binary Evolution of the Microquasar LS 5039*, *ApJ* **568** (2002) L27 [astro-ph/0201457].

[12] V. Bosch-Ramon and J.M. Paredes, *A numerical model for the γ-ray emission of the microquasar LS 5039*, *A&A* **417** (2004) 1075 [astro-ph/0401260].

[13] C.D. Dermer and M. Böttcher, *Gamma Rays from Compton Scattering in the Jets of Microquasars: Application to LS 5039*, *ApJ* **643** (2006) 1081 [astro-ph/0512162].

[14] V. Bosch-Ramon, M.V. Barkov and M. Perucho, *Orbital evolution of colliding star and pulsar winds in 2D and 3D: effects of dimensionality, EoS, resolution, and grid size*, *A&A* **577** (2015) A89 [1411.7892].

[15] V. Bosch-Ramon, *Properties of a hypothetical cold pulsar wind in LS 5039*, *A&A* **645** (2021) A86 [2012.11578].

[16] V. Bosch-Ramon and D. Khangulyan, *Understanding the Very-High Emission from Microquasars*, *Int. J. Mod. Phys. D* **18** (2009) 347 [0805.4123].

[17] E.V. Derishev and F.A. Aharonian, *A model for gamma-ray binaries, based on the effect of pair production feedback in shocked pulsar winds*, in *American Institute of Physics Conference Series*, F.A. Aharonian, W. Hofmann and F.M. Rieger, eds., vol. 1505 of *American Institute of Physics Conference Series*, pp. 402–405, Dec., 2012, DOI [1606.01073].